Supporting Information

The Mechanism of Isobutanal-Isobutene Prins Condensation Reactions on Solid Brønsted Acids

Shuai Wang and Enrique Iglesia*

Department of Chemical and Biomolecular Engineering, University of California at Berkeley, Berkeley, CA 94720 USA

* Corresponding author: iglesia@berkeley.edu

S1. Number of protons and Lewis acid sites on aluminosilicate samples

Titrations with 2,6-di-tert-butylpyridine (DTBP) during catalysis (described in Section 2.3 of the main text) were used to measure accessible proton sites on aluminosilicate samples (Table S1). The difference between the total amount of Al atoms (Al_{tot}, determined by elemental analysis) and the amount of Brønsted acid sites (H^+, determined by DTBP titrations) of each aluminosilicate sample was then used to estimate the content of Lewis acid sites (Al_{ex}; Table S1).

Table S1. The number of protons and Lewis acid sites on the aluminosilicate samples used in this study.

	H-CD-FAU	H-Al-MCM-41	H-ASA
H^+/Al_{tot}	0.37 [a]	0.35 [b]	0.025 [c]
Al_{ex}/Al_{tot}	0.63	0.65	0.975

[a] adapted from ref [25]; [b] adapted from Figure 2b; [b] adapted from Figure S7a.

S2. A top view of the aluminosilicate slab model.

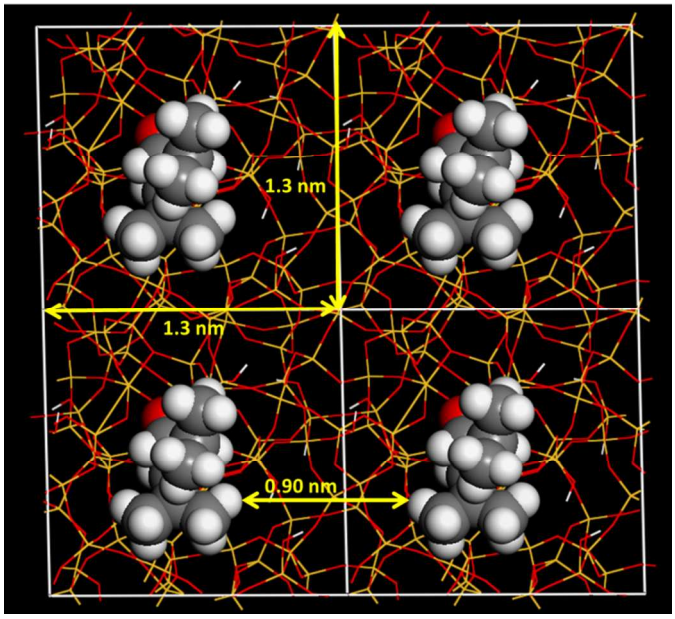

Figure S1. A top view of the isobutanal-isobutene Prins condensation C-C coupling transition state in an aluminosilicate unit cell (2 × 2 cells shown). The van der Waals radii for organic atoms are used to illustrate the occupied volume of the transition states.

S3. Structure of cluster models constructed from aluminosilicate slabs

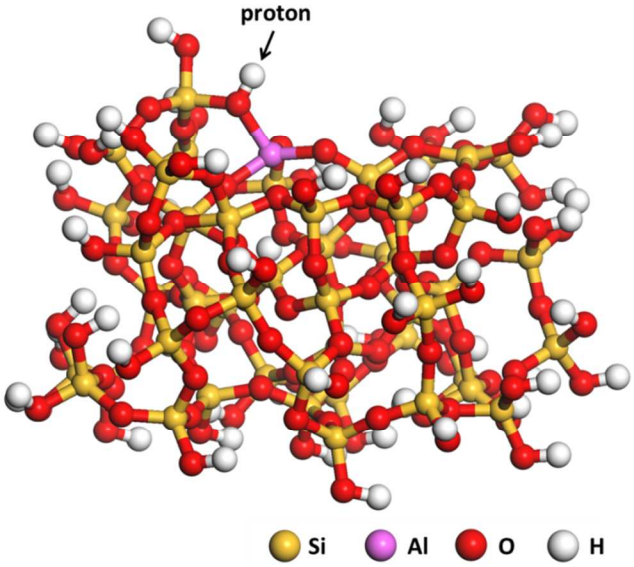

Figure S2. DFT-optimized structure of aluminosilicate cluster models ($Si_{47}AlO_{122}H_{53}$) constructed from the aluminosilicate slabs ($Si_{59}AlO_{12}4H_9$; Section 2.4). The proton used for the calculation of deprotonation energy is indicated.

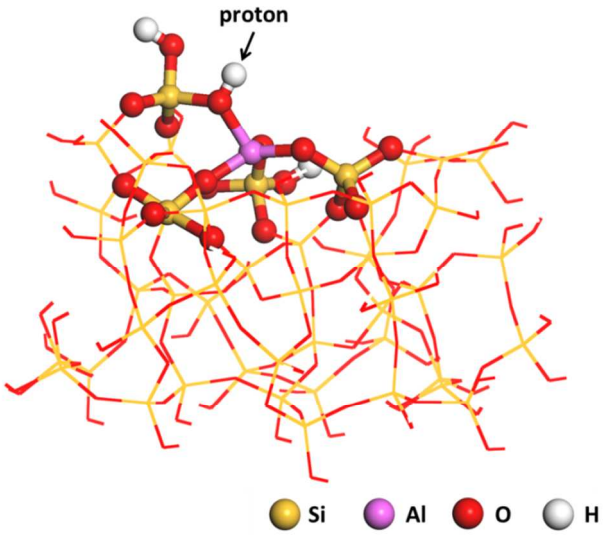

Figure S3. H^+-$[Al(OSiO_3H)_2(OSiO_3)_2]^-$ structure of the $Si_{47}AlO_{122}H_{53}$ cluster model (displayed in ball-and-stick modes; Fig. S1). All atoms in the H^+-$[Al(OSiO_3H)_2(OSiO_3)_2]^-$ structure are allowed to relax during geometry and energy optimizations of the cluster and its conjugate anion, whereas the other atoms in the cluster are frozen instead.

S4. Independence of formation rate ratios of regioisomers for each diene/alkene product on space velocity (using 2,5-dimethyl-hexadienes (2,5-DMH) and 2,4,4-trimethyl-pentenes (2,4,4-TMP) as illustrative examples for diene and alkene products, respectively)

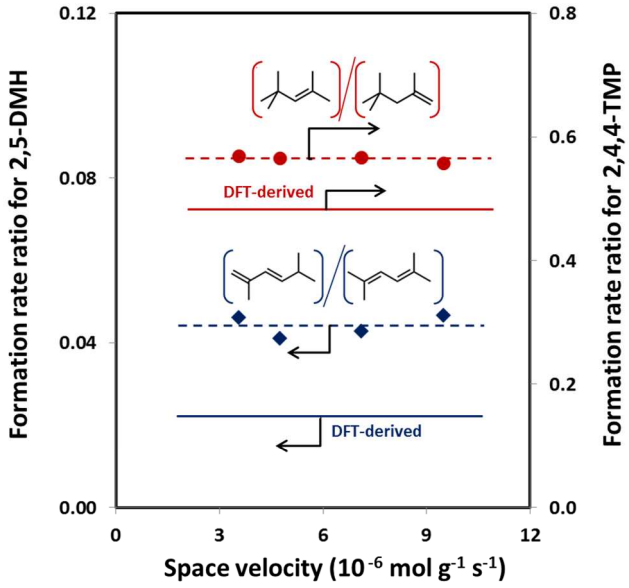

Figure S4. Formation rate ratios for trans-2,5-dimethyl-hexa-1,3-diene and 2,5-dimethyl-hexa-2,4-diene and for 2,4,4-trimethyl-pent-2-ene and 2,4,4-trimethyl-pent-1-ene as a function of space velocity (H-CD-FAU; 473 K; 1.0 kPa isobutanal; 0.5 kPa isobutene).

Dashed lines indicate linear trends. Solid lines represent DFT-derived rate ratios (G4MP2, 473 K, 1 bar).

S5. Conversion-selectivity relation for isobutanal-isobutene reactions on amorphous SiO_2-Al_2O_3 (H-ASA)

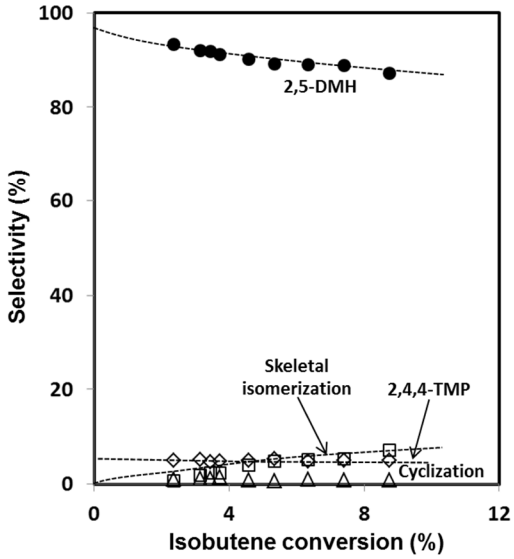

Figure S5. Selectivities of 2,5-DMH (●) and respective skeletal (□) and cyclized (Δ) isomers and 2,4,4-TMP (◊) as a function of isobutene conversion (H-ASA; 473 K; 2.0 kPa isobutanal; 1.0 kPa isobutene). Dashed curves indicate trends.

S6. Site titrations during isobutanal-isobutene reactions on H-ASA and $Nb_2O_5 \cdot nH_2O$

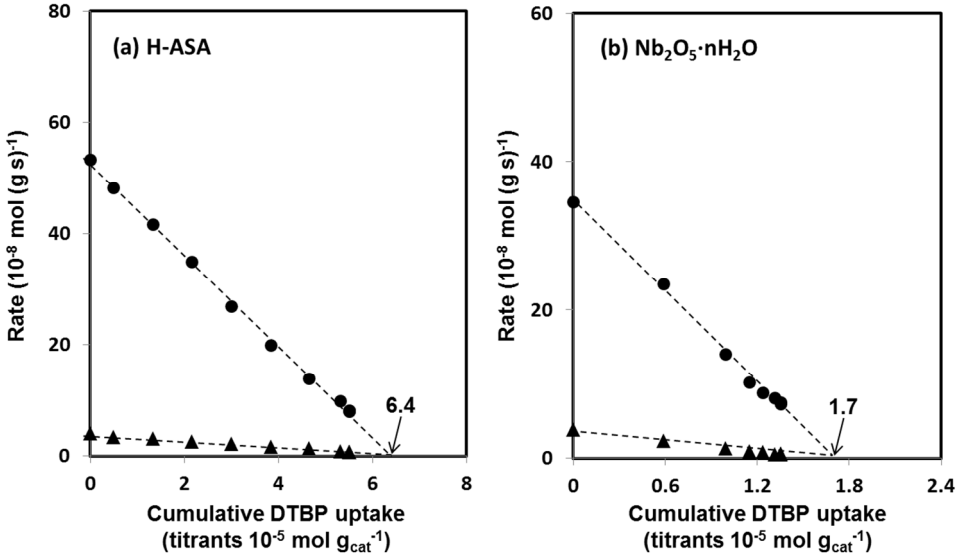

Figure S6. Isobutanal-isobutene Prins reaction (r_{prins}) and isobutene oligomerization (r_{oligo}) rates as a function of cumulative 2,6-di-tert-butylpyridine (DTBP) uptakes on (a)

H-ASA and (b) $Nb_2O_5 \cdot nH_2O$ (473 K; 2.0 kPa isobutanal; 1.0 kPa isobutene; DTBP 2 Pa for H-ASA and 10 Pa for $Nb_2O_5 \cdot nH_2O$). Dashed lines represent linear regression fits.

S7. Deactivation of solid acids during Prins condensation and oligomerization reactions

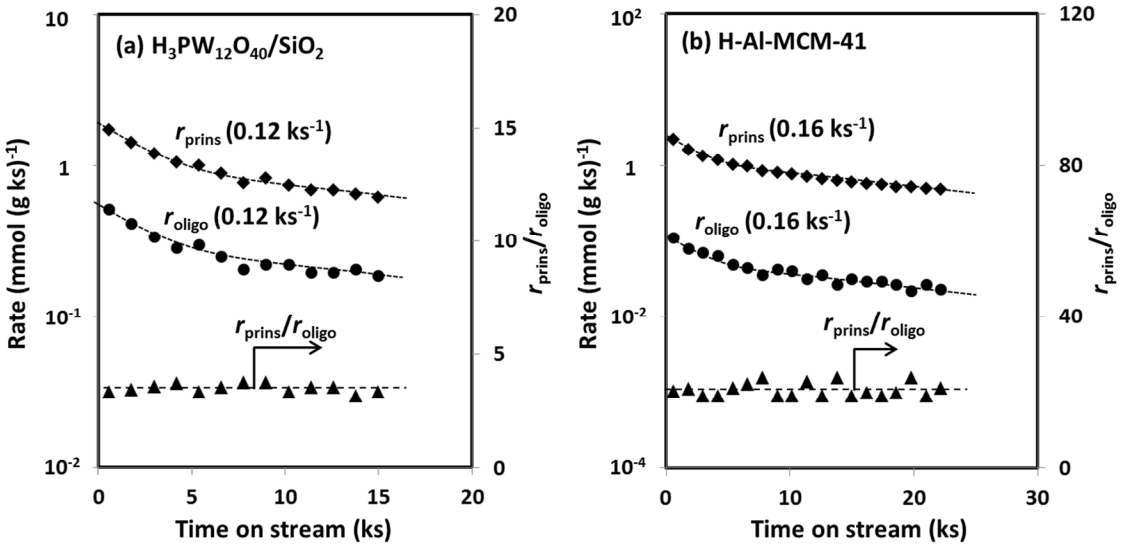

Figure S7. Semi-logarithmic plots of isobutanal-isobutene Prins condensation and isobutene oligomerization rates as a function of time-on-stream (a) on $H_3PW_{12}O_{40}/SiO_2$ and (b) on H-Al-MCM-41 (473 K, 2.0 kPa isobutanal, 1.0 kPa isobutene). First-order deactivation constants are shown in parenthesis. Dashed curves indicate qualitative trends.

S8. Parity plots for measured and predicted rates of isobutanal-isobutene reactants on solid acids

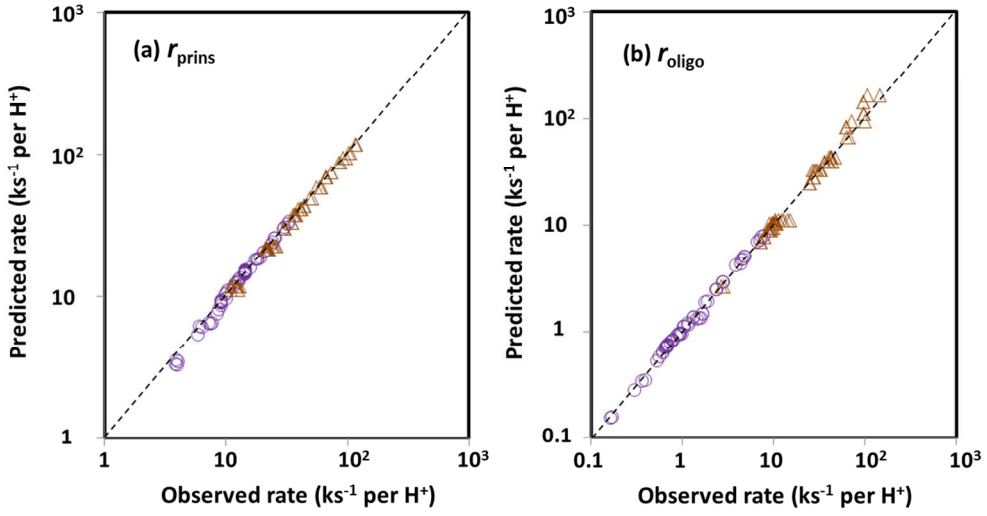

Figure S8. Parity plots for the measured and predicted rates of (a) isobutanal-isobutene Prins condensation (Eq. 2) and (b) isobutene oligomerization (Eq. 3) on H-Al-MCM-41

(○) and $H_3PW_{12}O_{40}/SiO_2$ (Δ) with the regression-fitted parameters shown in Table 3 of the main text.

S9. DFT estimates for stability of monomeric adsorbed species on POM clusters

Table S2. DFT-derived adsorption enthalpies (ΔH_{ads}) and adsorption free energies (ΔG_{ads}) for adsorbed species formed from isobutanal and isobutene on proton sites of POM clusters as illustrated in Scheme 8.[a]

	POM cluster	Isobutanal-derived species		Isobutene-derived species		
		H-bonded isobutanal	1-hydroxy-iso-butoxide	π-complex	iso-butoxide	tert-butoxide
ΔH_{ads} (kJ mol^{-1})	$H_5AlW_{12}O_{40}$	-78	-64	-60	-68	-54
	$H_4SiW_{12}O_{40}$	-79	-68	-60	-64	-49
	$H_2SW_{12}O_{40}$	-84	-66	-64	-61	-44
ΔG_{ads} (kJ mol^{-1})	$H_5AlW_{12}O_{40}$	-9	28	0	10	32
	$H_4SiW_{12}O_{40}$	-12	25	1	16	39
	$H_2SW_{12}O_{40}$	-13	27	-3	19	44

[a] PBE+D3BJ; 473 K, 1 bar; relative to a bare cluster and respective gaseous reactants.

S10. DFT-derived enthalpies for intermediates and transition states involved in Prins condensation and oligomerization pathways on aluminosilicates

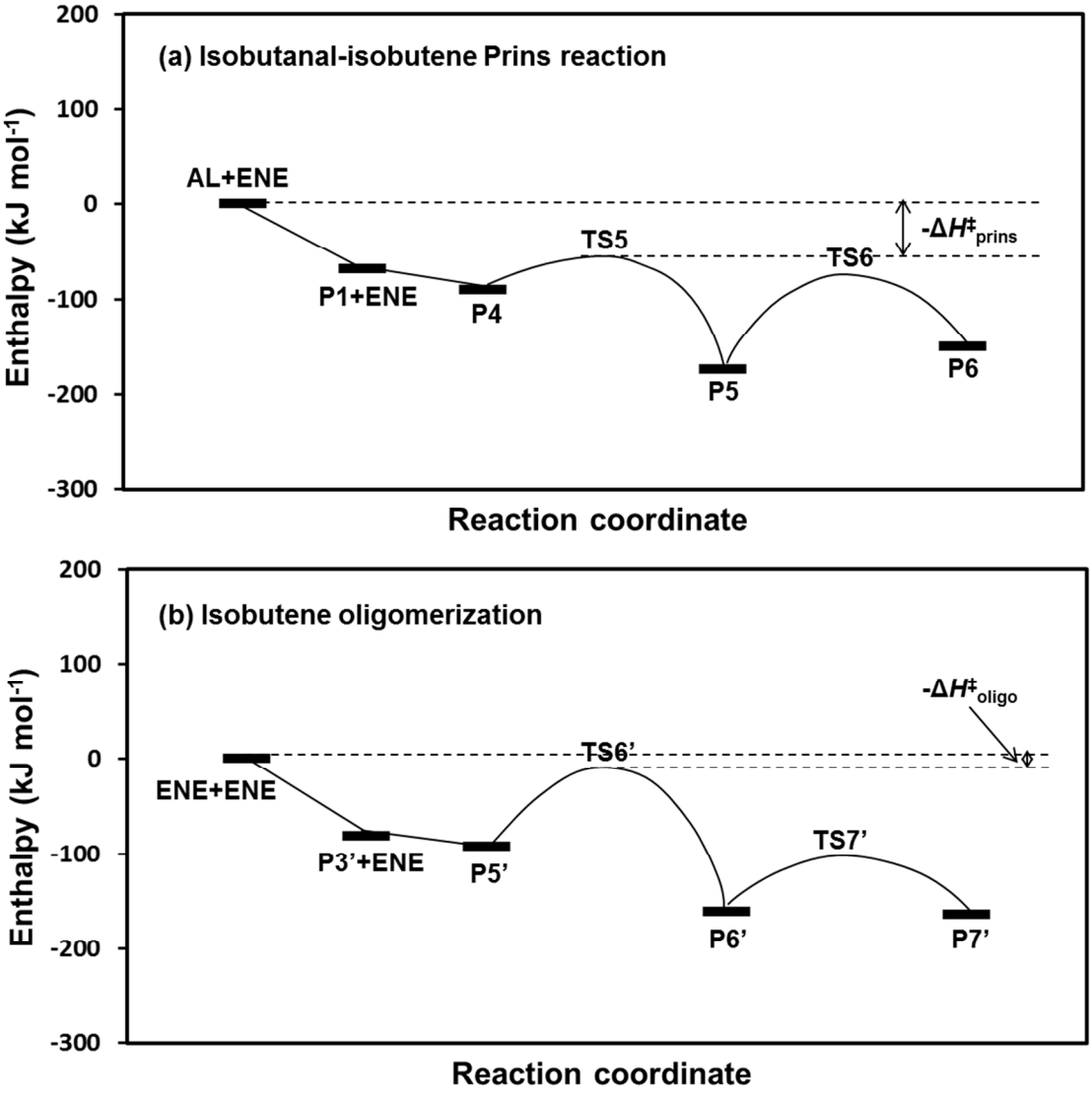

Figure S9. DFT-derived reaction enthalpy diagrams of (a) isobutanal-isobutene Prins condensation and (b) isobutene oligomerization pathways (aluminosilicate ($Si_{59}AlO_{124}H_9$) slabs, PBE+D3BJ; 473 K, 1 bar). TSj and Pj represent respective transition state and product of Step j in Scheme 5; AL and ENE represent gaseous isobutanal and isobutene, respectively. Energies are relative to a bare surface and respective gaseous reactants.

S11. DFT-derived enthalpies and free energies for intermediates and transition states involved in Prins condensation and oligomerization pathways on POM clusters

Table S3. DFT-derived enthalpies (*H*) and free energies (*G*) for intermediates and transition states involved in isobutanal-isobutene Prins condensation elementary steps on POM clusters.[a]

	POM cluster	Prins condensation pathway[b]				
		P4	TS5	P5	TS6	P6
H (kJ mol^{-1})	$H_5AlW_{12}O_{40}$	-90	-27	-123	-91	-137
	$H_4SiW_{12}O_{40}$	-95	-38	-120	-90	-141
	$H_3PW_{12}O_{40}$	-98	-46	-118	-99	-147
	$H_2SW_{12}O_{40}$	-100	-49	-119	-97	-147
G (kJ mol^{-1})	$H_5AlW_{12}O_{40}$	22	114	45	81	11
	$H_4SiW_{12}O_{40}$	17	103	47	81	8
	$H_3PW_{12}O_{40}$	13	96	50	73	2
	$H_2SW_{12}O_{40}$	12	93	49	74	1

[a] PBE+D3BJ; 473 K, 1 bar; relative to a bare cluster, a gaseous isobutanal molecule and a gaseous isobutene molecule. [b] TSj and Pj represent respective transition state and product of Step j in Scheme 5a.

Table S4. DFT-derived enthalpies (*H*) and free energies (*G*) for intermediates and transition states involved in isobutene oligomerization elementary steps on POM clusters.[a]

	POM cluster	Oligomerization pathway[b]				
		P5'	TS6'	P6'	TS7'	P7'
H (kJ mol^{-1})	$H_5AlW_{12}O_{40}$	-64	-18	-154	-101	-94
	$H_4SiW_{12}O_{40}$	-63	-31	-151	-108	-95
	$H_3PW_{12}O_{40}$	-61	-39	-149	-110	-96
	$H_2SW_{12}O_{40}$	-59	-44	-150	-112	-95
G (kJ mol^{-1})	$H_5AlW_{12}O_{40}$	76	121	8	53	30
	$H_4SiW_{12}O_{40}$	77	108	11	46	29
	$H_3PW_{12}O_{40}$	79	100	14	45	29
	$H_2SW_{12}O_{40}$	81	95	13	42	29

[a] PBE+D3BJ; 473 K, 1 bar; relative to a bare cluster, two gaseous isobutene molecules. [b] TSj and Pj represent respective transition state and product of Step j in Scheme 5b.

S12. DFT-derived entropy components in activation free energies for isobutanal-isobutene Prins condensation and isobutene oligomerization reactions on solid acids

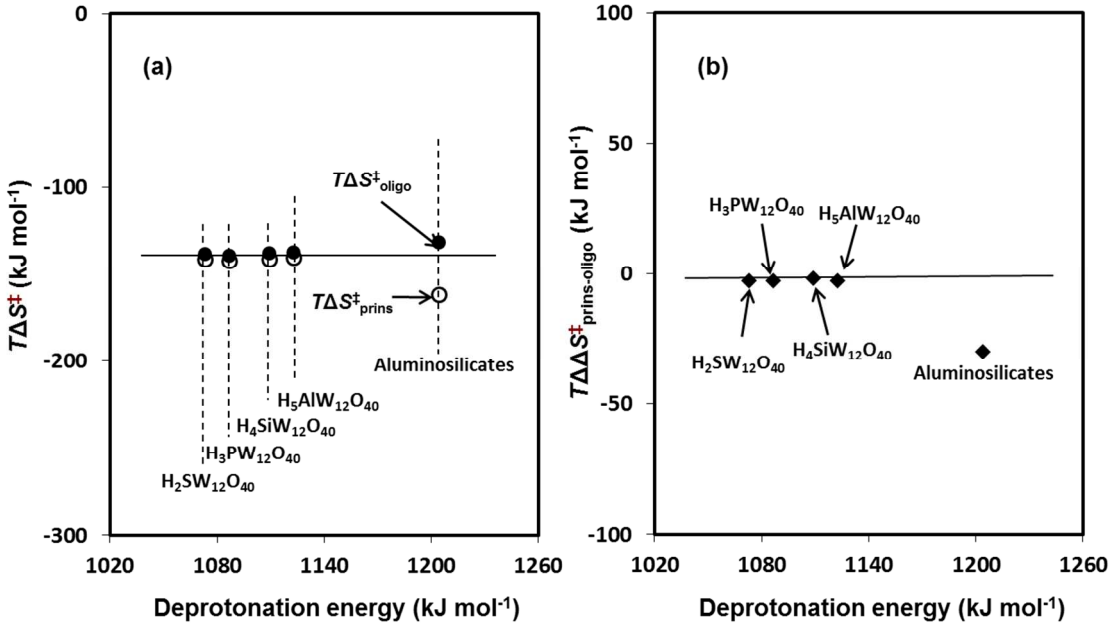

Figure S10. DFT-derived (a) entropy components in activation free energies for isobutanal-isobutene Prins condensation and isobutene oligomerization ($T\Delta S^{\ddagger}_{prins}$ and $T\Delta S^{\ddagger}_{oligo}$) and (b) their respective difference ($T\Delta\Delta S^{\ddagger}_{prins-oligo}$) as a function of deprotonation energy of solid acids (PBE+D3BJ; referenced to a bare proton site and respective gaseous reactants; 473 K, 1 bar). Solid lines represent trends.